Metal-Metal Bonding in Engel-Brewer Intermetallics: "Anomalous" Charge Transfer in $ZrPt_3$

Hua Wang and Emily A. Carter*

Contribution from the Department of Chemistry and Biochemistry, University of California, Los Angeles, California 90024-1569. *Received July 9, 1992*

Abstract: Ab initio generalized valence bond, configuration interaction, and multiconfiguration self-consistent field calculations have been performed to examine the properties of the early-late transition metal bimetallic cluster $ZrPt_3$, as a representative model of Engel-Brewer compounds. Such intermetallic compounds are known to be extremely thermally stable in the bulk form. We find the atomization energy of the $ZrPt_3$ cluster at its bulk geometry to be at least 101.1 kcal/mol, which supports the Engel-Brewer suggestion that an alloy of Zr and Pt should be particularly stable. However, we find that the charge transfer occurs in the opposite direction from that assumed by the Engel-Brewer theory; namely, the Zr atom is predicted to donate approximately one electron to the three Pt atoms. The high thermal stability of these compounds is attributed to a combination of localized, highly polar, sd-sd bonds between Zr and Pt that enhance the normal metallic (sp-sp) bonding present in homometallic Pt clusters. In order to better understand intermetallic metal-metal bonding and charge transfer, calculations for low-lying states of ZrPt dimer have also been carried out. Bond energies, vibrational frequencies, equilibrium geometries, and charge distributions are predicted.

I. Introduction

Materials that exhibit high thermal stability and resistance to oxidation and corrosion are extremely desirable, as protective coatings for mechanical systems and for catalysts of endothermic reactions, both of which may be required to operate at elevated temperatures. Appropriate alloys of transition metals might possibly serve as both highly stable catalysts and as thermally stable, oxidation-resistant protective coatings. Engel-Brewer intermetallic compounds show potential to serve as such materials.

Engel-Brewer compounds are those that have been shown to obey the empirical theory developed by Engel and Brewer.[1] By applying the Pauling valence-bond approach to transition metal systems, Engel postulated a correlation between metal electron configurations and crystal structures. The theory states that the crystal structures of metals and their intermetallic compounds are determined by the number of valence s and p electrons, as in the Hume-Rothery rules for nontransition metals. For example, Engel suggested that the body-centered cubic (bcc) structure correlated with $d^{n-1}s^1$ (where n is the total number of valence electrons) and that the hexagonal close-packed (hcp) and face-centered cubic (fcc) structures corresponded to $d^{n-2}s^1p^1$ and $d^{n-3}s^1p^2$ electron configurations, respectively. Although d-electrons were thought to contribute greatly to bonding and cohesion, they were suggested to have only an indirect role in determining the crystal structure. Brewer extended this idea and successfully predicted multicomponent phase diagrams[2] and thermodynamic activities for many transition metal alloys.[2-4] The most important aspect of these Engel-Brewer compounds, as far as we are concerned, is the unusual cohesive energy postulated to be the result of d-electron interactions. The most stable intermetallic compounds were proposed[1c,3,4] to be group 4 (e.g., Hf, Zr)-group 9/10 (e.g., Ir, Pt) alloys, in which the group 9/10 metal was postulated to donate electrons to the empty d-orbitals of the group 4 metal, in order to maximize the number of d-d bonds. In the case of Zr-Pt alloys, the Engel-Brewer model predicts that they are extremely stable at high temperature because of transfer of roughly two d-electrons from Pt (fcc, $d^7s^1p^2$) to unoccupied valence orbitals of Zr (bcc, d^3s^1), allowing the formation of five intermetallic d-d bonds. Only scant experimental data exist for the thermodynamic properties of these intermetallic compounds;[4-6] however, the high melting point and large negative free energies of formation certainly confirm the stability of these alloys. For $ZrPt_3$, its melting point and standard Gibbs energy of formation were measured to be 2390-2470 K (congruent melting)[4] and -128 kJ/g-atom, respectively.[5]

As far as we are aware, previous related quantum chemical studies have been limited to early-late intermetallic dimers involving Pd or Ni with Sc or Y.[7] We have investigated both a dimer and tetramer of Zr and Pt as model Engel-Brewer intermetallics and describe herein the physical properties and charge-transfer characteristics that appear responsible for the unusual stability of these compounds. Generalized valence bond, configuration interaction, and multiconfiguration self-consistent field calculations for ZrPt and $ZrPt_3$ were performed. From these calculations, we extract a description for ZrPt including its electronic spectrum, equilibrium bond lengths, bond energies, vibrational frequencies, and metal-metal bond character of a number of low-lying electronic states. We also predict the electronic spectrum, the cohesive energy, and metal-metal bond character for $ZrPt_3$ at its bulk geometry. In particular, our objective is to understand the origin of this compound's stability and to test the validity of the Engel-Brewer model of bonding.

II. Calculational Details

A. Zr and Pt Atoms. The 10 valence electrons of Pt were treated explicitly within the (3s3p3d/3s2p2d) Gaussian basis set of Hay and Wadt with the core electrons represented by the associated relativistic effective core potential (RECP).[8a] Twelve electrons (four valence and the eight outermost s and p core electrons) on Zr were described within a (8s5p4d/4s3p2d) Gaussian basis set using a similar RECP.[8b] This RECP includes the effect of the mass-velocity and Darwin terms in the relativistic Hamiltonian, leading to physically realistic relativistic orbital contractions. This orbital shrinkage is the dominant chemical relativistic effect, since such contractions change the orbital overlaps within bonds, thereby affecting the intrinsic bond strength and character. However, this RECP neglects spin-orbit interactions. Thus, the results presented here may be considered as averaged over total angular momentum states.

B. ZrPt Dimer. The equilibrium geometries (optimized by point-by-point interpolation) and self-consistent wave functions for all states of ZrPt were obtained by complete active space MCSCF (CASSCF) calculations,[9] where the CAS included all 14 valence electrons (10 from Pt and 4 from Zr) within all 12 valence orbitals (2 s and 10 d orbitals).

(1) (a) Engel, N. *Acta Metall.* **1967**, *15*, 557. (b) Brewer, L. *Acta Metall.* **1967**, *15*, 553. (c) Brewer, L. *Science* **1968**, *161*, 115.
(2) Brewer, L. In *High-Strength Materials*; Zackay, Ed.; Wiley: New York, 1965; pp 12-103.
(3) Gibson, J. K.; Brewer, L.; Gingerich, K. A. *Metall. Trans. A* **1984**, *15A*, 2075.
(4) Brewer, L.; Wengert, P. R. *Metall. Trans.* **1973**, *4*, 83.
(5) Srikrishnan, V.; Ficalora, P. J. *Metall. Trans.* **1974**, *5*, 1471.
(6) Meschter, P. J.; Worrell, W. L. *Metall. Trans. A* **1977**, *8A*, 503.
(7) (a) Shim, I.; Gingerich, K. A. *Chem. Phys. Lett.* **1983**, *101*, 528. (b) Faegri, K., Jr.; Bauschlicher, C. W., Jr. *Chem. Phys.* **1991**, *153*, 399.
(8) (a) Hay, P. J.; Wadt, W. R. *J. Chem. Phys.* **1985**, *82*, 270. (b) Hay, P. J.; Wadt, W. R. *J. Chem. Phys.* **1985**, *82*, 299.
(9) (a) Yaffe, L. G.; Goddard, W. A., III *Phys. Rev. A* **1976**, *13*, 1682. (b) Roos, B. O. In *Ab Initio Methods in Quantum Chemistry*, 2; Lawley, K. P., Ed.; Wiley: New York, 1987.

0002-7863/93/1515-2357$04.00/0

Our CASSCF calculations were restricted to C_{2v} symmetry, and we solved for the lowest root of each symmetry. Thus, we present only the lowest energy solution for each spin and spatial symmetry and do not rule out the possibility that other states of the same symmetry may also be low-lying. All possible singlet, triplet, and quintet states in C_{2v} symmetry were examined. Septet states, which correspond to no low-spin coupling between Zr and Pt, were expected to be unbound and hence were not examined. We put a restriction in the MCSCF calculation on the maximum number of open shells allowed per configuration, allowing up to 6 instead of the 10 possible. Test calculations on the $^1A_1$ and $^5B_1$ states with both 6 open shells and the unrestricted case with 10 open shells showed little difference for either the wave functions or the energies (ΔE (6 open − 10 open) is 1.3 kcal/mol for the ^1A state and 2.5 kcal/mol for the $^5B_1$ state). Since the 10 open-shell MCSCF case for the triplet was prohibitively expensive (70 500 spin eigenfunctions for the $^3A_1$ state), and the 6 open-shell restriction introduces only small errors in the energy, it appears that we can glean essentially the same information with less computational cost.

C. $ZrPt_3$ Tetramer. Different treatments were utilized for the electronic states of $ZrPt_3$ due to the increased size of the system. We optimized wave functions and obtained energy splittings at the GVB-PP-(5/10) level.[10] GVB-PP(5/10) indicates that five electron pairs are correlated as GVB pairs, with two natural orbitals per pair, for a total of 10 correlated electrons. PP stands for perfect-pairing, i.e., each pair of electrons is singlet-coupled. The correlated electrons consist of the four valence electrons on Zr and the open-shell s- and d-electrons on each Pt atom. This active space on the Pt_3 moiety is the same as that used in a previous study of Pt_3 itself.[13]

The GVB-RCI(5/10) wave function allows both single and double excitations within each GVB pair, leading to a total of $3^5 = 243$ configurations. This level of calculation optimizes both spin–coupling and interpair correlations. The GVB-CI(5/10) wave function includes all possible excitations within the 10 GVB correlated orbitals: i.e., this is a 10-electron full CI within the 10 GVB orbitals for a total of 8701 configurations and 29 700 spin eigenfunctions for the ^3A state. Finally, we also carried out GVBCI(5/10)-MCSCF calculations for the cohesive energy of the ground ^3A state and the first excited ^1A state, where MCSCF indicates we optimized the orbitals self-consistently for the GVB-CI(5/10) wave function (i.e., this is a 10-electron, 10 orbital CASSCF calculation). Note that the GVB wave function is stabilized via localization of the correlated electron pairs. This necessarily lowers the symmetry of the exact molecular wave function to a wave function with no symmetry in this particular case. For example, in $ZrPt_3$ we find three localized Zr–Pt bonds in the GVB description that do not correspond to symmetry-adapted functions, yet this wave function has a much lower energy than one forced to adopt the full symmetry of the molecule. This type of "symmetry-breaking" will occur in all but the simplest variationally optimized valence bond wave functions. It essentially corresponds to the fundamental difference between a local, valence bond picture and a symmetry-adapted linear combination of atomic orbitals–molecular orbitals (LCAO–MO) view.

All calculations for all of the electronic states of the $ZrPt_3$ cluster were performed for one of the two bulk structures, which is an equilateral triangular pyramid (a distorted tetrahedron possessing C_{3v} symmetry), with the Zr atom at the apex ($R_{Pt-Pt} = 2.812$ Å and $R_{Zr-Pt} = 2.818$ Å).[11] The bulk crystal structure of $ZrPt_3$ is hexagonal close-packed, with 16 atoms in the unit cell.[11]

D. Comparison of ZrPt and $ZrPt_3$. Ideally, we would have preferred to carry out full-valence CASSCF calculations on $ZrPt_3$ as we did on ZrPt, but as stated above, this was prohibitively expensive and thus the less complete GVBCI-MCSCF wave function was employed for $ZrPt_3$. In some sense, we were fortunate that $ZrPt_3$ had easily identifiable electron pairs to correlate within the GVB scheme. Given our desire to compare results from ZrPt and $ZrPt_3$ calculations, it is sensible to suggest at least carrying out the same lower level calculations on ZrPt that were performed on $ZrPt_3$. We indeed tried this but, unlike $ZrPt_3$, the higher $C_{\infty v}$ symmetry of ZrPt led to too many orbital degeneracies and no obvious unique pairing schemes for the GVBCI-MCSCF. As a result of these degeneracies, GVBCI-MCSCF is a poor approximation for the ZrPt dimer. These results are not reported because they do not represent an adequate solution for the electronic wave function. Hence we are forced to consider only qualitative comparisons between the ZrPt and $ZrPt_3$ results.

Table I. Atomic State Splittings of Zr and Zr^+ (kcal/mol)

species	state	ΔE(expt)[a]	ΔE[GVB-RCI][b]
Zr^+	^4F (d^3)	178.9	132.2
Zr^+	^4F (d^2s^1)	163.3	124.9
Zr	^5D (d^4)	63.2	58.1
Zr	^5F (d^3s^1)	13.6	2.4
Zr	^3F (d^2s^2)	0.0	0.0[c]

[a] Experimental values are averaged over J states.[12] [b] GVB-RCI(1/2) results for the ^3F state using the (4s3p2d) basis set and the RECP of Hay and Wadt.[8] The corresponding levels of calculation for the ^5D, ^5F (for Zr), and ^4F (both d^3 and d^2s^1 for Zr^+) states are open-shell HF. [c] The total energy of the ^3F state at the GVB-RCI(1/2) level is −45.984 70 hartrees.

Table II. Atomic State Splittings of Pt and Pt^- (kcal/mol)

species	state	ΔE(expt)[a]	ΔE[GVB-RCI][b]
Pt	^1D (d^9s^1)	32.1	23.1
Pt	^3F (d^8s^2)	14.7	16.0
Pt	^1S (d^{10})	11.0	22.3
Pt	^3D (d^9s^1)	0.0	0.0[c]
Pt^-	^2D (d^9s^2)	−59.6 ± 2.9	−16.6

[a] Experimental values are averaged over J states.[12,14] [b] GVB-RCI-(1/2) results for the ^1S state using the (3s2p2d) basis set and the RECP of Hay and Wadt.[8] The corresponding levels of calculation for the ^1D, ^3F and ^3D states are open shell HF. The Pt^- calculation was carried out at the GVB-RCI(1/5) level, where the s-electron pair was described by two s and three p natural orbitals. [c] The total energy of the ^3D state at the open-shell HF level is −26.238 10 hartrees.

III. Results and Discussion

A. Zr, Zr^+, Pt, and Pt^-. The atomic state splittings of Zr and Zr^+ described by the Hay–Wadt basis set and RECP are compared with experiment in Table I.[12] The lowest level calculation that avoids biases in orbital occupation and in spin–coupling involves a GVB-RCI(1/2) on the ^3F state of Zr (s/p_z correlation) and restricted open-shell Hartree–Fock (HF) calculations on all other states; we combine these together in the table as a GVB-RCI(1/2) set of calculations. For Zr atom, GVB-RCI(1/2) calculates the correct ground state, but predicts the ^5F (d^3s^1) state to be too stable, leading to a bias favoring both high-spin and enhanced d-character in the Zr wave function. While the predicted ionization potentials are substantially lower than experiment, they are still extremely large and should at least qualitatively predict properly the ease of charge transfer (vide infra). The Zr^+ d^3–d^2s^1 state splitting is lower than the experimental value by 8.3 kcal/mol, leading to a bias toward enhanced d-character in Zr^+. These biases will be accounted for in our $ZrPt_x$ studies.

Table II shows the Pt atomic state splittings for the Hay–Wadt basis set and RECP. The GVB-RCI(1/2) set of calculations includes GVB-RCI(1/2) (d/d* correlation) on the ^1S state of Pt and restricted open-shell HF on all other states. Compared with experimental results,[12] GVB-RCI(1/2) predicts the correct ground state and good ^3F–^3D splittings. The ^1S–^3D splitting at the GVB-RCI(1/2) level results in a bias against d^{10}-character in the wave function for Pt clusters at this low level of theory. The Pt anion is bound at the GVB(1/5)-PP level, but the electron affinity is too small by over a factor of 3. Given that the Pt basis set has no diffuse functions and hence was not optimized for a negative ion, we are not surprised to find poor quantitative agreement with experiment. This merely means that our basis set will probably underestimate any charge transfer to Pt (vide infra).

B. ZrPt Dimer. Twelve low-lying electronic states of ZrPt were determined by CASSCF calculations in the C_{2v} point group. As mentioned above, we solved for the lowest energy quintet, triplet, and singlet states of A_1, A_2, B_1, and B_2 symmetry. Table III

(10) The details of GVB theory may be found in: (a) Hunt, W. J.; Dunning, T. H., Jr.; Goddard, W. A., III *Chem. Phys. Lett.* **1969**, *3*, 606. (b) Goddard, W. A., III; Dunning, T. H., Jr.; Hunt, W. J. *Chem. Phys. Lett.* **1969**, *4*, 231. (c) Hunt, W. J.; Goddard, W. A., III; Dunning, T. H., Jr. *Chem. Phys. Lett.* **1970**, *6*, 147. (d) Hunt, W. J.; Hay, P. J.; Goddard, W. A., III *J. Chem. Phys.* **1972**, *57*, 738. (e) Bobrowicz, F. W.; Goddard, W. A., III In *Methods of Electronic Structure Theory*; Schaefer, H. F., Ed.; Plenum: New York, 1977; pp 79–127.

(11) Villars, P.; Calvert, L. D. *Pearson's Handbook of Crystallographic Data for Intermetallic Phases*; American Society for Metals: Metals Park, OH, 1985; p 3065.

(12) Moore, C. E. In *Atomic Energy Levels As Derived From the Analyses of Optical Spectra*; U.S. Government Printing Office: Washington, DC, 1971.

Table III. Dominant Orbital Occupancies for the 12 Low-Lying Electronic States of Each Symmetry for ZrPt at the CASSCF Level[a]

	orbital occupancies											
states	a_1	a_1	a_1	a_1	b_1	b_1	b_2	b_2	a_1	a_1	a_2	a_2
$^5A_1$	2	2	1	0	2	0	1	1	2	1	2	0
$^5A_2$	2	2	1	0	1	0	2	1	2	1	2	0
$^5B_1$	2	2	1	0	2	0	2	1	2	1	1	0
$^5B_2$	2	2	1	0	2	0	2	1	1	1	2	0
$^3A_1$	2	2	1	0	2	0	2	0	2	1	2	0
$^3A_2$	2	2	1	0	1	0	2	1	2	1	2	0
$^3B_1$	2	2	1	0	2	0	2	1	2	1	1	0
$^3B_2$	2	2	0	0	2	0	2	1	2	1	2	0
$^1A_1$	2	2	2	0	2	0	2	0	2	0	2	0
$^1A_2$	2	2	2	0	2	0	2	0	2	1	1	0
$^1B_1$	2	2	1	0	2	0	2	1	2	1	1	0
$^1B_2$	2	2	1	0	2	0	2	1	2	0	2	0

[a] The first set of a_1 orbitals in the list are either pure σ orbitals or mixtures of σ and δ that mix under C_{2v} symmetry. The second set of a_1 orbitals are mixtures of σ and δ also. The b_1 and b_2 orbitals are pure π orbitals, while the a_2 orbitals are pure δ.

Table IV. Equilibrium Properties of 12 Electronic States of ZrPt from CASSCF Calculations[a]

state	R_e[b] (Å)	ω_e[b] (cm^{-1})	D_e[c] (kcal/mol)	config/SEF[d]
$^1B_1$	2.83	179	30.8	13888/34496
$^1A_2$	2.68	187	34.2	13888/34496
$^3A_2$	2.90	142	36.4	13888/55104
$^5A_2$	2.89	147	37.7	10528/23968
$^5A_1$	2.87	152	39.6	9996/25116
$^3B_1$	2.77	161	47.3	13888/55104
$^1B_2$	2.43	295	48.4	13888/34996
$^5B_1$	2.76	171	48.8	10528/23968
$^5B_2$	2.75	171	50.7	10528/23968
$^3B_2$	2.47	250	59.4	13888/55104
$^1A_1$	2.38	348	62.8	14568/35904
$^3A_1$	2.37	313	80.9	13776/56448

[a] Calculated at the 14 electrons in 12 orbitals CASSCF level (see text). [b] R_e is the equilibrium bond length in angstroms; ω_e is the harmonic vibrational frequency in wavenumbers. [c] D_e is the equilibrium bond dissociation energy in kcal/mol. The CASSCF total energy for the $^3A_1$ state is −72.351 79 hartrees. The corresponding total energies for Zr and Pt are −45.984 70 and −26.238 10 hartrees, respectively. [d] Config is the number of spatial configurations; SEF is the number of spin eigenfunctions.

Table V. CASSCF Mulliken Populations for the 12 Electronic States of ZrPt

state	atom	s	p	d	total
$^1B_1$	Zr	3.31	6.43	1.84	11.58
	Pt	1.38	0.26	8.78	10.42
$^1A_2$	Zr	3.28	6.40	1.77	11.45
	Pt	1.60	0.28	8.67	10.55
$^3A_2$	Zr	2.87	6.45	2.48	11.80
	Pt	1.37	0.29	8.54	10.20
$^5A_2$	Zr	2.89	6.45	2.45	11.79
	Pt	1.37	0.29	8.55	10.21
$^5A_1$	Zr	2.90	6.43	2.16	11.49
	Pt	1.39	0.32	8.80	10.51
$^3B_1$	Zr	3.15	6.33	2.16	11.65
	Pt	1.35	0.28	8.72	10.35
$^1B_2$	Zr	2.76	6.06	2.08	10.90
	Pt	1.63	0.13	9.34	11.10
$^5B_1$	Zr	3.14	6.33	2.17	11.64
	Pt	1.35	0.27	8.74	10.36
$^5B_2$	Zr	3.15	6.33	2.18	11.66
	Pt	1.31	0.27	8.76	10.34
$^3B_2$	Zr	2.63	6.03	2.43	11.09
	Pt	1.40	0.09	9.42	10.91
$^1A_1$	Zr	3.11	6.14	2.34	11.59
	Pt	1.43	0.10	8.88	10.41
$^3A_1$	Zr	2.82	6.26	1.83	10.91
	Pt	1.62	0.19	9.28	11.09

displays the dominant configuration for each state. While it is typical for workers in this field to calculate CI or MCSCF wave functions in abelian subgroups of the full symmetry group of the molecule (for ease of computation),[7b] this approach is not always rigorously correct for linear molecules unless additional constraints are imposed, such as those described for the CASSCF calculations in ref 7b. As can be seen from Table III, all of the states that we have considered are "symmetry-broken", except for the $^1A_1$ state which is fortuitously a pure $^1\Sigma^+$ eigenstate under the full $C_{\infty v}$ symmetry. In other words, we have solved for states that possess C_{2v} symmetry, while the actual molecule possesses $C_{\infty v}$ symmetry. Given the qualitative discussion of bonding with which we are primarily concerned, these C_{2v} eigenstates will suffice for our purposes. Thus, a quantitatively correct description would require a more complex CASSCF wave function in which pure $C_{\infty v}$ eigenstates were constructed; however, that is beyond the scope or purpose of the present work.

Table IV lists the equilibrium properties found for these 12 low-lying electronic states. The equilibrium bond lengths range from 2.37 Å to 2.90 Å, while the vibrational frequencies vary from 142 cm^{-1} to 348 cm^{-1} and the bond energies range from 30.8 kcal/mol to 80.9 kcal/mol. In general, the higher spin states exhibit larger bond lengths and smaller vibrational frequencies. This is especially true for the quintet states. The extent of charge transfer also appears to be higher for the lower spin states, reaching a maximum of 1.1 electrons transferred for one of the singlet states ($^1B_2$, Table V). The local atomic electron configuration tends to be approximately s^1d^2 Zr^+ and s^2d^9 Pt^- for the most polar states (consistent with the known ground states of the atomic ions), while the more covalent states tend to be approximately s^1d^3 Zr and s^1d^9 Pt. The bias in the Zr basis toward enhanced d-character (s^1d^3) suggests that the more covalent states might in actuality be more s^2d^2-like on Zr. Indeed, some of the states that are half-covalent and half-ionic do exhibit more s^2d^2-like character.

Unlike our previous study of Pt clusters (Pt_2 and Pt_3),[13] ZrPt displays a well-separated electronic spectrum. We showed previously that weak d–d coupling was responsible for the high density of states found in Pt clusters. While stronger d–d coupling may play a role due to the larger size of the Zr d-orbitals compared with those of Pt, another important reason for the low density of states is the fundamentally different character of the bonding in this early–late intermetallic; it is primarily ionic, as discussed in more detail below. Bulk ionic materials tend to have large band gaps, which is consistent with the large energy splittings between states that we predict here.

The ground state of ZrPt is predicted to be a $^3A_1$ state, which exhibits the shortest bond length (2.37 Å), a large amount of charge transfer (1.09 electrons), and is bound by 80.9 kcal/mol (Tables IV and V). Since this state is not the pure $C_{\infty v}$ ground eigenstate (which could be $^3\Delta$ or $^3\Sigma$), this bond energy is a lower bound on the true ground-state bond energy. (The true $C_{\infty v}$ ground eigenstate is predicted to be $^3\Sigma^+$, based on the orbital occupations of the $^3A_1$ state shown in Table III and the lack of a $^3A_2$ state degenerate with $^3A_1$, which would have been expected for a doubly degenerate $^3\Delta$ state.) By contrast, Pt_2 at a similar level of theory[13]

(13) Wang, H.; Carter, E. A. *J. Phys. Chem.* **1992**, *96*, 1197.
(14) Hotop, H.; Lineberger, W. C. *J. Phys. Chem. Ref. Data* **1985**, *14*, 731.

is only bound by 26.7 kcal/mol. Part of the explanation for the factor of 3 difference between the homometallic dimer and the heterometallic dimer bond strength may lie in noticing that the predicted ZrPt bond length is 0.38 Å shorter than the sum of the metallic radii of Zr and Pt, while the predicted Pt_2 bond length[13] is actually longer than twice the metallic radius of Pt. The shortened bond length in ZrPt will strengthen overlap-sensitive (and hence bond-length-sensitive) d–d bonds relative to Pt_2, which will increase the overall bond strength. Perhaps even more important than enhanced d–d bonding is ionic contributions to the bonding, which will also increase the bond strength as the bond length decreases. Ionic bonding is clearly an important component of the bonding in this dimer, since substantial d- and s-electron transfers occur in the ground state of ZrPt. Recall that Engel and Brewer[1] suggested charge-transfer-induced enhancements in d–d bonding as the origin of the unusual stability of heterometallics. However, the Engel–Brewer proposal is to transfer roughly two electrons from Pt to Zr to create formally Zr^{2-} (s^1d^5) and Pt^{2+} ($s^1p^2d^5$), followed by formation of five d–d bonds between Zr and Pt. First, we find that the local electron configurations on Zr and Pt are approximately $s^{0.5}p^{0.5}d^{2-3}$ and $s^{1-2}d^9$, respectively, which are not the same as the electron configurations postulated by Engel and Brewer. Second, while a large degree of electron transfer does occur between Zr and Pt (0.2–1.1 electrons, Table V), the electrons are transferred *from Zr to Pt*, rather than Pt to Zr, as in the Engel–Brewer model. Thus, in contrast to Engel–Brewer theory, electrostatic interactions in the opposite direction (but in the same direction with what would be expected from their relative work functions) contribute greatly to the extreme stability of ZrPt dimer.

With regard to possible errors in the ordering of the electronic states, we suggested in section II that this Zr basis set is biased by ~11 kcal/mol (at the RCI level) toward high spin and that this Pt basis set is biased against low spin, even though the correct ground states of the atoms are predicted. We remain confident in our prediction of the ground state of ZrPt as a triplet, since the first excited state is ~18 kcal/mol higher at the CASSCF level. Since the error in the atomic state splittings should decrease with increasing electron correlation and CASSCF wave functions contain more electron correlation, this 11-kcal/mol bias is likely to be an upper bound to the error in our ZrPt calculations. Thus, since $\Delta E(^1A_1-^3A_1)$ is large compared to the error, a triplet state ($^3\Sigma^+$) is most probably the ground state. Given the overall bias toward high spin present in the basis set, it may be that the ordering of some of the higher-lying states may shift, with some of the singlet and triplet states dropping below some of the quintet states. Since our goal was primarily to predict qualitative properties of the ground state, we leave such issues to future studies.

Concerning the accuracy of the predicted ground-state properties, we should consider how reliable we expect the charge-transfer characteristics to be. In particular, we suggest that the extent of charge transfer is probably modelled nearly correctly, despite absolute errors in the calculations of the ionization potential (IP) of Zr and the electron affinity (EA) of Pt. This is because the extent of charge transfer is largely determined by the *difference* between the IP and the EA. If we compare the experimental versus theoretical IP(Zr) – EA(Pt), the experimental value is 103.7 ± 2.9 kcal/mol, while the theoretical value is 108.3 kcal/mol. Thus, the extent of charge transfer should be predicted reasonably well, because the errors have fortuitously cancelled.

C. $ZrPt_3$. In order to understand how to approach the electronic structural properties and chemical bonding in $ZrPt_3$, we began our study by first investigating the electronic structure of low-lying states of Pt_3. The cluster was assumed to have an equilateral triangle geometry with R(Pt–Pt) = 2.812 Å, identical with Pt_3 configurations in bulk hcp $ZrPt_3$. Table VI summarizes three levels of GVB/CI calculations performed on the nine lowest-lying electronic states of each symmetry in the C_{2v} point group. Theoretical methods for determining the wave functions for the lowest-lying states were described in our earlier work on Pt_3.[13] The $^7A_1$ state with all six open-shell electrons unpaired (i.e., no metal–metal bonds) is unbound by 11.4 kcal/mol with respect to three ground-state ^3D Pt atoms at the GVB-CI(3/6) level. The nine states ($^3B_2$, $^3B_1$, $^5A_2$, $^3A_2$, $^5B_1$, $^1A_1$, $^5A_1$, $^5B_2$, and $^3A_1$) are found to be within about 3 kcal/mol of the ground state for all three levels, with $^3A_1$ being the ground state. As mentioned previously, the high density of states of different spin lying so close to the ground state is due to the fact that sp–sp bonding is the dominant force which holds the cluster together, and d–d interactions are almost negligible,[13] due to the dramatic shrinkage of the size of d-orbitals in the late transition metals compared to the early ones.

Table VI. Relative Energies (kcal/mol) for Nine Low-lying States of Pt_3 in the Equilateral Triangle Geometry (θ = 60.0° and R_{Pt-Pt} = 2.812 Å)

	ΔE (kcal/mol)		
state	GVB-PP(3/6)	GVB-RCI(3/6)	GVB-CI(3/6)
$^3B_2$	2.3	2.4	2.5
$^3B_1$	3.1	2.1	2.3
$^5A_2$	1.9	2.0	2.2
$^3A_2$	3.1	2.1	2.1
$^5B_1$	1.9	2.0	2.1
$^1A_1$	2.2	1.0	1.6
$^5A_1$	0.8	0.7	1.5
$^5B_2$	0.0	0.06	0.3
	(−78.757 57)[a]		
$^3A_1$	1.0	0.0	0.0
		(−78.757 68)[a]	(−78.759 40)[a]

[a] The total energy in hartrees is given in parentheses underneath ΔE for the ground state at each level of calculation.

Table VII. Relative Energies (kcal/mol) for Six Low-Lying Electronic States of $ZrPt_3$ in Its Bulk Geometry (R_{Pt-Pt} = 2.812 Å, R_{Zr-Pt} = 2.818 Å)

	ΔE (kcal/mol)			
state	GVB-PP-(5/10)	GVB-RCI-(5/10)	GVB-CI-(5/10)	D_e (kcal/mol)[b]
$^9A''$	24.5	25.6	29.4	
$^9A'$	23.0	25.3	27.8	
^7A	15.6	16.8	18.4	
^5A	11.1	11.8	12.1	
^1A	5.1	4.9	4.3	97.1
^3A	0.0	0.0	0.0	101.1
	(−124.839 50)[a]	(−124.843 34)[a]	(−124.850 59)[a]	

[a] The total energy in hartrees is given in parentheses underneath ΔE for the ground state at each level of calculation. [b] D_e is obtained from a GVB-CI(5/10)-MCSCF calculation.

We obtained wave functions at the GVB-PP(5/10) level for low-lying electronic states of $ZrPt_3$ by examining the interaction of Zr atom in its ground state (valence electron configuration $4d^25s^2$) and first excited state (valence electron configuration $4d^35s^1$) with the low-lying states of Pt_3. These fragment states lead naturally to a set of six intermediate and low-spin states of $ZrPt_3$. The energy splittings of the six low-lying electronic states calculated at three different correlation levels are given in Table VII. The nonet spin states were calculated within the C_s point group, while the rest of the states were optimized with no symmetry to allow possible localization of correlated electron pairs (as discussed in section II.C). Increasing the level of electron correlation increases the energy splittings, from a range of 24.5 kcal/mol at the GVB-PP(5/10) level to 29.4 kcal/mol at the GVB-CI(5/10) level, but it does not change the ordering of any of the states. We also see from Table VII that the higher spin states are at higher energy, except for the ^3A and ^1A states. However, the ^3A–^1A splitting is decreased by increasing the level of calculation, from 5.1 kcal/mol at the GVB-PP(5/10) level to 4.3 kcal/mol at the GVB-CI(5/10) level. In order to determine the ^3A–^1A energy splitting and the atomization energy of $ZrPt_3$ tetramer to higher accuracy, we also optimized the shape of the orbitals for the GVB-CI(5/10) wave function in a GVB-CI(5/10)*MCSCF calculation. The ^3A–^1A splitting is found to be 4.0 kcal/mol, almost unchanged from the GVB-CI(5/10) calculation.

Table VIII. GVB-PP Mulliken Populations[a] for Six Electronic States of $ZrPt_3$

state	atom	s	p	d	total
$^9A''$	Zr	2.62	6.50	2.21	11.33
	Pt1	1.01	0.33	8.86	10.20
	Pt2	1.09	0.30	8.85	10.24
	Pt3	1.09	0.30	8.85	10.24
$^9A'$	Zr	2.61	6.50	2.21	11.32
	Pt1	1.13	0.31	8.82	10.26
	Pt2	1.04	0.31	8.86	10.21
	Pt3	1.04	0.31	8.86	10.21
^7A	Zr	2.28	6.25	2.52	11.05
	Pt1	0.94	0.37	8.94	10.25
	Pt2	1.11	0.25	9.01	10.37
	Pt3	1.30	0.22	8.81	10.33
^5A	Zr	2.51	6.64	2.00	11.15
	Pt1	0.80	0.20	9.33	10.33
	Pt2	0.79	0.20	9.33	10.32
	Pt3	1.05	0.36	8.78	10.19
^1A	Zr	2.58	6.67	1.94	11.19
	Pt1	0.79	0.18	9.37	10.33
	Pt2	0.73	0.18	9.37	10.28
	Pt3	0.70	0.17	9.33	10.20
^3A	Zr	2.53	6.67	1.98	11.18
	Pt1	0.79	0.18	9.35	10.32
	Pt2	0.73	0.18	9.37	10.28
	Pt3	0.71	0.18	9.33	10.22

[a] Mulliken populations were obtained by summing over both natural orbitals of each GVB pair.

The atomization energy of the $ZrPt_3$ tetramer (the ^3A state) at its bulk geometry was found to be 101.1 kcal/mol with respect to separated Zr (^3F) and Pt (^3D) atoms. This predicted $ZrPt_3$ atomization energy will be a lower bound at the GVB-CI (5/10)*MCSCF level, since this level of calculation only involved 8701 spatial configurations and 29 700 spin eigenfunctions for the ^3A state. The full-valence CI MCSCF (CASSCF) calculations analogous to the ones carried out for ZrPt dimer are beyond of the scope of our computational facilities at the moment, since this would have involved a 34-electron 24-orbital CASSCF. However, this large lower bound on the atomization energy at least strongly suggests that this early–late intermetallic cluster is thermally stable, consistent with the Engel–Brewer ideas.

In the case of $ZrPt_3$, the charge transfer is again found to occur in the opposite direction from the Engel–Brewer prediction; namely, Zr atom donates 0.67–0.95 electron to Pt_3 in the six low-lying electronic states (Table VIII). The high degree of ionicity is again probably the main cause of the unusual thermal stability in these intermetallic compounds. As stated earlier, we believe the extent of charge transfer is being modelled reasonably, since the predicted difference in IP and EA is correct to within 4 out of 104 kcal/mol (vide supra). Notice also the large extent of s–p hybridization: if Zr and Pt were not utilizing valence p-character in their bonds, then the p-electron populations in Table VIII would be 6 for Zr (the outer core electrons included in our calculation) and 0 for Pt. The Zr atom is roughly $s^{0.5}p^{0.5}d^2$ Zr^+ in these states, while the Pt atoms are roughly $s^1p^{0.3}d^9$ $Pt^{-0.2-0.3}$. The need for s–p hybridization has been noted before in metal clusters: intermetallic bonds involve interstitial orbitals that can only form via substantial s–p mixing.[13,15]

Table IX displays the bonding and hybridization character found for the active orbitals of the ground (^3A) and first excited (^1A) states. For the ^3A state, both of the singly-occupied orbitals are localized on Zr, with one electron in a d-orbital and the other one in a primarily sp-hybridized orbital. The four high overlap GVB pairs in the ^3A state include one Pt–Pt s–s bond (overlap = 0.82) with two electrons delocalized within the Pt_3 base and three highly ionic, highly localized Zr–Pt d–d bonds (overlap = 0.64), with each Pt atom involved in one of the three bonds. The ^1A state has four GVB pairs that are very similar to those in the ^3A state. However, the ^1A state has one more very low overlap GVB pair (overlap = 0.005) which is simply a singlet coupling

(15) McAdon, M. H.; Goddard, W. A., III *J. Phys. Chem.* **1987**, *91*, 2607.

Table IX. Mulliken Populations for the Active Orbitals of Two Low-Lying States of $ZrPt_3$

state	orbital	atom	s	p	d
^3A	GVB pair 1	Zr	0.08	0.06	0.20
		Pt1	0.20	0.06	1.41
		Pt2	0.00	0.00	0.00
		Pt3	0.00	0.00	0.00
	GVB pair 2	Zr	0.08	0.06	0.19
		Pt1	0.00	0.00	0.00
		Pt2	0.24	0.06	1.39
		Pt3	0.00	0.00	0.00
	GVB pair 3	Zr	0.09	0.06	0.22
		Pt1	0.00	0.00	0.00
		Pt2	0.00	0.00	0.00
		Pt3	0.22	0.06	1.36
	GVB pair 4	Zr	0.03	0.02	0.01
		Pt1	0.39	0.06	0.78
		Pt2	0.29	0.05	0.10
		Pt3	0.19	0.02	0.06
	open-shell 1	Zr	0.00	0.00	0.98
		Pt1	0.00	0.00	0.00
		Pt2	0.00	0.00	0.00
		Pt3	0.00	0.00	0.01
	open-shell 2	Zr	0.27	0.48	0.22
		Pt1	0.00	0.01	0.00
		Pt2	0.00	0.01	0.00
		Pt3	0.00	0.00	0.00
^1A	GVB pair 1	Zr	0.08	0.06	0.19
		Pt1	0.20	0.06	1.42
		Pt2	0.00	0.00	0.00
		Pt3	0.00	0.00	0.00
	GVB pair 2	Zr	0.08	0.06	0.19
		Pt1	0.00	0.00	0.00
		Pt2	0.23	0.06	1.39
		Pt3	0.00	0.00	0.00
	GVB pair 3	Zr	0.08	0.05	0.24
		Pt1	0.00	0.00	0.00
		Pt2	0.00	0.00	0.00
		Pt3	0.22	0.06	1.37
	GVB pair 4	Zr	0.04	0.01	0.02
		Pt1	0.39	0.07	0.79
		Pt2	0.28	0.05	0.09
		Pt3	0.18	0.02	0.06
	GVB pair 5	Zr	0.30	0.50	1.16
		Pt1	0.01	0.01	0.01
		Pt2	0.00	0.00	0.00
		Pt3	0.00	0.01	0.01

of those two open-shell orbitals that were present in the ^3A state. Since these orbitals are easily orthogonalized to each other, electron–electron repulsion may favor a ^3A ground state. However, given that the calculations on Zr and Zr^+ indicated a slight basis set bias in favor of high-spin states and that the high-spin electrons in ^3A $ZrPt_3$ are localized on Zr (see Table IX), it may be that the ground state is actually ^1A. We also find that $ZrPt_3$ retains the same type of Pt–Pt bonding in the Pt_3 moiety as in the bare Pt_3 cluster,[13] namely, that sp–sp interactions also play an important role in the formation of the $ZrPt_3$ cluster.

Finally, the amount of charge transfer can be independently evaluated in a qualitative sense by examining the orbitals comprising the bonds between Zr and Pt. Figure 1 displays contour plots of the overlapping GVB orbitals for one of the (correlated) Zr–Pt bonds in the $ZrPt_3$ cluster. The orbital in each panel of this figure contains one electron and the asterisks represent the locations of the nuclei, with the lower nucleus being Pt. This bond is highly ionic, because more than one electron is localized on Pt. However, we do see that there is a contribution of sd–sd hybrid bonding between Zr and Pt in the left one-electron orbital. The right one-electron orbital is an sd hybrid completely localized on Pt. Thus it is clear that both ionic and sd–sd bonding contribute to the overall stability of this intermetallic compound.

IV. Conclusions

In this work, we predict a $^3\Sigma^+$ ground state for ZrPt, which is bound by a minimum of 80.9 kcal/mol. All 12 electronic states examined for ZrPt have bond energies larger than the homo-

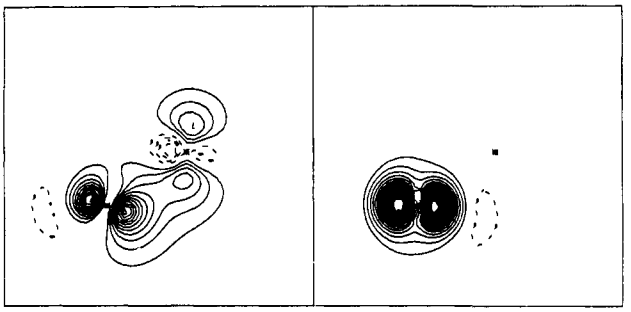

Figure 1. Contour plots of the two singlet-paired GVB-PP one-electron orbitals of a Zr–Pt bond. Solid lines represent positive contours while dashed lines represent negative contours. Contours are plotted every 0.04 au, ranging from −0.4 to +0.4 au. The asterisks represent nuclei, with one Pt atom at the lower left and the Zr atom to the right of center. The right panel shows an electron localized on Pt in an sd hybrid orbital, while the left panel shows an electron delocalized via an sd–sd interaction between Zr and Pt. This illustrates a superposition of sd–sd bonding and ionic bonding, since more than one electron is localized on Pt.

metallic dimer Pt_2 at the same level of theory. The states are split to a much greater degree than in the homometallic case, which we propose is due to the ionic nature of the bonding, as well as perhaps an increase in d–d interactions. These states all show a high degree of ionicity in the opposite direction from Engel–Brewer theory, with electrostatic interactions found to be at least as important as sp–sp or d–d metallic bonding. The electronic spectrum for $ZrPt_3$ at its bulk geometry shows a much lower density of states than in the homometallic Pt_3 cluster, indicating again that the bonding interactions are quite different. However, two states are very low-lying; the ^1A and ^3A states are separated by only 4 kcal/mol, making it difficult to predict, because of basis set biases, which state is the true ground state. The atomization energy of our predicted ground ^3A state is at least 101.1 kcal/mol, which suggests great thermal stability for the clusters as well as the bulk material. Significant electron transfer occurs from Zr to Pt_3 that is again contradictory to the assumptions in Engel–Brewer theory. Both localized electrostatic interactions as well as some sd–sd hybrid bonding between Zr and the three Pt atoms and the normal metallic sp–sp bonding within the Pt_3 moiety are found to be the important components in the formation of $ZrPt_3$.

In sum, these ab initio calculations suggest that bulk intermetallic compounds are more stable than their homometallic counterparts, but not because of pure d–d interactions and electron transfer from the late transition metal to the early transition metal as suggested previously.[1-4] Rather, the enhanced stability is due to electron transfer from the early transition metal to the late transition metal (which should have been expected based on their work functions) combined with sd–sd and sp–sp metallic interactions between the heterometallic and homometallic components of the alloy, respectively.

Acknowledgment. This work was supported by the Air Force Office of Scientific Research. E.A.C. acknowledges additional support from the National Science Foundation and the Camille and Henry Dreyfus Foundation via Presidential Young Investigator and Dreyfus Teacher–Scholar Awards, respectively.

Y-Conjugated Compounds: The Equilibrium Geometries and Electronic Structures of Guanidine, Guanidinium Cation, Urea, and 1,1-Diaminoethylene

Alberto Gobbi and Gernot Frenking*

Contribution from the Fachbereich Chemie, Philipps-Universität Marburg, Hans-Meerwein-Strasse, D-3550 Marburg, Germany. *Received July 24, 1992*

Abstract: Ab initio calculations at the MP2/6-31G(d) level of theory predict that the equilibrium geometries of the Y-conjugated compounds guanidine (**1**), guanidinium cation (**2**), urea (**5**), and 1,1-diaminoethylene (**6**) are nonplanar. **1**, **5**, and **6** have energy minimum structures with strongly pyramidal amino groups. The equilibrium geometry of the guanidinium cation **2b** has D_3 symmetry; the planar amino groups are rotated by ~15° out of the D_{3h} form **2a**. The planar structure **2a** becomes lower in energy than **2b** when corrections are made for zero-point vibrational energies. The observed planar geometries of guanidine and urea in the crystal are probably caused by hydrogen bonding. The resonance stabilization of the Y-conjugated structures is not very high, because the rotation of one amino group leaves a subunit which is isoelectronic to the allyl anion. Yet, resonance stabilization in the Y-conjugated forms is important, as it is revealed by the calculated rotational barriers for the NH_2 groups and the substantial lengthening of the C–NH_2 bonds upon rotation. The energy difference between 1,1-diaminoethylene (**6**) and 1,2-diaminoethylene (**7**) is mainly due to conjugative stabilization in **6**. The two isomers have nearly the same energy when one amino group in **6** is rotated. The calculated proton affinity of guanidine is only 237.7 kcal/mol. It is concluded that the very high basicity of **1** in solution is not caused by the resonance stabilization of **2**, but rather by strong hydrogen bonding of the guanidinium cation.

1. Introduction

The structure and properties of guanidine (**1**) and its associated acid, the guanidinium cation (**2**) (Figure 1), has attracted the interest of theoretical chemists for many decades.[1-9] Guanidine is one of the strongest organic bases (pK_a = 13.6)[10] known in chemistry, and guanidine and its derivatives are biologically and industrially important chemicals.[11] In fact, until the synthesis of the so-called "proton sponges",[12,13] **1** was considered *the* strongest organic base.

(1) Pauling, L. *The Nature of the Chemical Bond*, 3rd ed.; Cornell University Press: Ithaca, NY, 1960; p 286.
(2) Gund, P. *J. Chem. Educ.* **1972**, *49*, 100.
(3) Kollman, P.; McKelvey, J.; Gund, P. *J. Am. Chem. Soc.* **1975**, *97*, 1640.
(4) Capitani, J. F.; Pedersen, L. *Chem. Phys. Lett.* **1978**, *54*, 547.
(5) Sapse, A. M.; Massa, L. J. *J. Org. Chem.* **1980**, *45*, 719.
(6) Ohwada, T.; Itai, A.; Ohta, T.; Shudo, K. *J. Am. Chem. Soc.* **1987**, *109*, 7036.
(7) Sreerama, N.; Vishveshwara, S. *J. Mol. Struct.* **1989**, *194*, 61.
(8) Williams, M. L.; Gready, J. E. *J. Comput. Chem.* **1989**, *10*, 35.
(9) Wiberg, K. B. *J. Am. Chem. Soc.* **1990**, *112*, 4177.
(10) Angyal, S. J.; Warburton, W. K. *J. Chem. Soc.* **1951**, 2492.
(11) *The Chemistry of Guanidine*; American Cyanamid Co.: Wayne, NJ, 1950.
(12) Alder, R. W.; Bryce, M. R.; Goode, N. C.; Miller, N.; Owen, J. *J. Chem. Soc., Perkin Trans. 1* **1981**, 2840.
(13) Staab, H. A.; Saupe, T. *Angew. Chem.* **1988**, *100*, 895; *Angew. Chem., Int. Ed. Engl.* **1988**, *27*, 865.

0002-7863/93/1515-2362$04.00/0